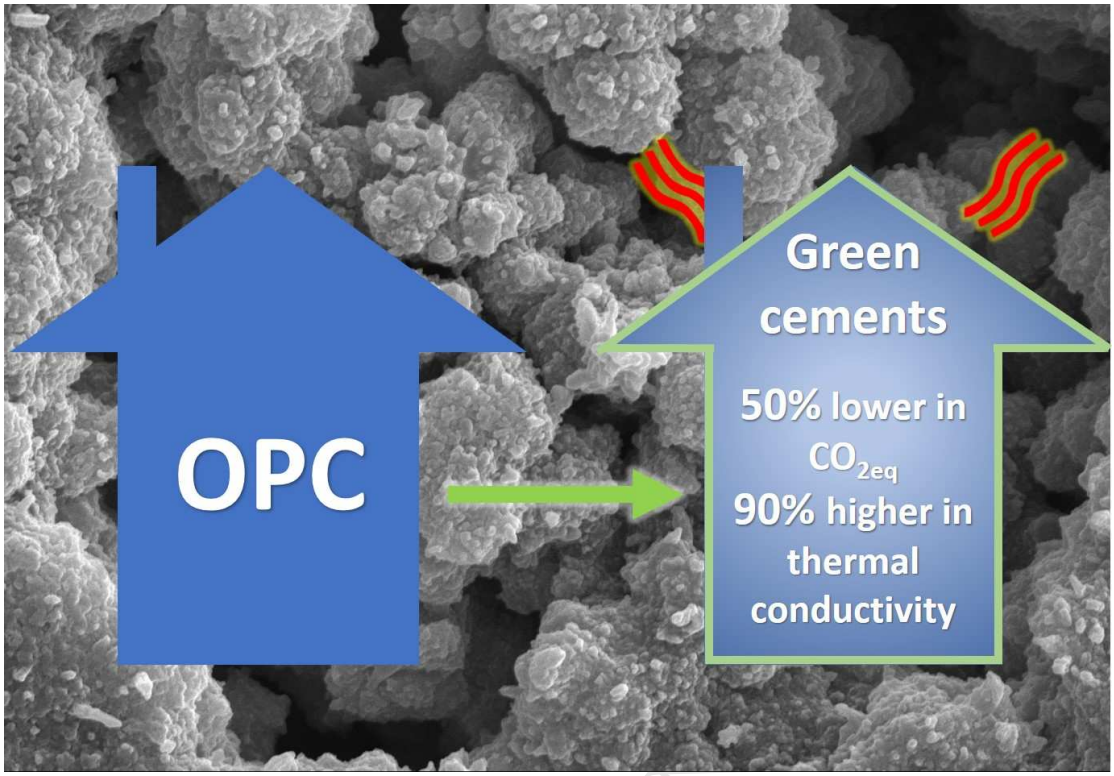

wordcount: 5020 words, 9 Figures, 3 Tables

Can Portland cement be replaced by low-carbon alternative materials? A study on thermal properties and carbon emissions of innovative cements

Riccardo Maddalena[a], Jennifer J. Roberts[a], Andrea Hamilton*[a]

[a] *University of Strathclyde, Department of Civil and Environmental Engineering, Glasgow G1 1XJ, UK*

**corresponding author: andrea.hamilton@strath.ac.uk*

Abstract

One approach to decarbonising the cement and construction industry is to replace ordinary Portland cement (OPC) with lower carbon alternatives that have suitable properties. We show that seven innovative cementitious binders comprised of metakaolin, silica fume and nano-silica have improved thermal performance compared with OPC and we calculate the full CO_2 emissions associated with manufacture and transport of each binder for the first time. Due to their high porosity, the thermal conductivity of the novel cements is 58–90% lower than OPC, and we show that a thin layer (20 mm), up to 80% lower than standard insulating materials, is enough to bring energy emissions in domestic construction into line with 2013 Building Regulations. Carbon emissions in domestic construction can be reduced by 20–50% and these cementitious binders are able to be recycled, unlike traditional insulation materials.

Keywords: cement industry, nano-silica, carbon footprint, thermal conductivity.

1. Introduction

Ordinary Portland cement (OPC) is one of the most manufactured materials in the world. Over 3 billion tonnes of cement were manufactured in 2012 [1], and global demand is expected to increase due to rapid infrastructural development of emerging economies [2, 3]. Indeed, global cement production is forecast to reach 3.7–4.4 billion tons by 2050, as stated by the World Business Council for Sustainable Development (WBCSD) report in 2009 [4]. Cement is primarily used by the construction and geotechnical industries, but there are other emerging applications, including nuclear waste containment, biological and dental ceramics, and water filtration. Cement clinker is produced by calcining limestone (or marl or chalk) with some clay in a furnace at *c.* 1500 °C and is a significant source of greenhouse gas emissions (GHG), which are usually expressed as CO_2 equivalent (CO_{2eq}) and sometimes referred to as "embedded carbon" [5]. Approximately 900 kg of CO_{2eq} is released per ton of cement produced by current practices [6]. Thus, the cement industry is estimated to contribute 5–7% of global anthropogenic CO_2 emissions in 2009 [7]. The direct release of CO_2 from calcination during clinker production is responsible for *c.* 50% of the emissions from cement manufacture (Figure 1). Much of the remaining emissions come from the combustion of fossil fuels for calcination, plus excavation, transportation, milling and grinding processes. Given the global effort to curb CO_2 emissions in an attempt to mitigate dangerous climate change effects [8] (for example the 2015 Paris Agreement, a framework for an internationally coordinated effort to tackle climate change), and the expected rise in global demand for cement, reducing emissions from cement manufacture presents an important challenge. Indeed, the 'decarbonisation' of cement production is becoming a more prominent issue for the cement sector, as evidenced by the WBCSD and International Energy Agency (IEA) Cement Roadmap (2009), the Industrial Decarbonisation & Energy Efficiency Roadmaps to 2050 report and British

Cement Association (BCA73 Carbon Strategy 2005) [4, 9, 10].

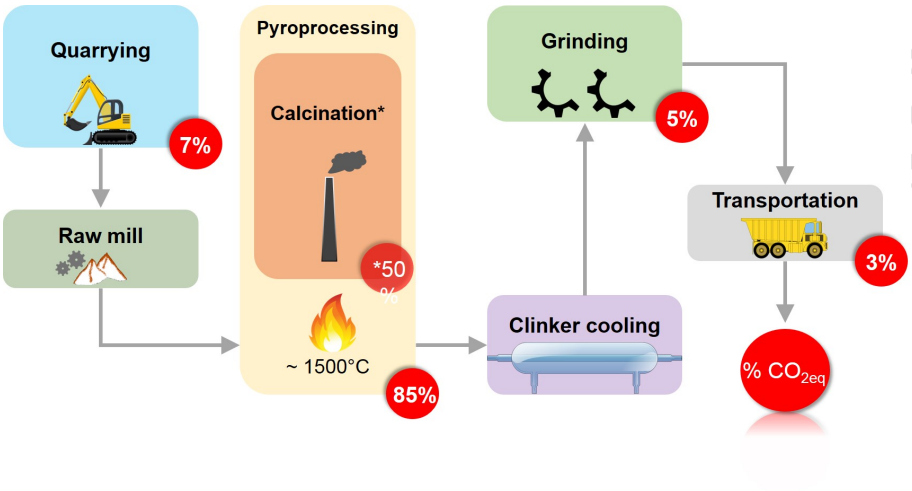

Figure 1: Simplified diagram of the cement production process. Red circles indicate the percentage of CO_{2eq} emissions associated with manufacturing. $^{(*)}$50% of the emissions associated with pyroprocessing arises from direct release of CO_2 from calcination and the remaining 35% from fuel and energy consumption. [Image adapted from Imbabi et al., (2012)[1]]

Researchers and industry have focused their attention on using alternative fuels in place of conventional fossil fuels (and so reducing the GHG emissions of the traditional OPC manufacturing process), and developing alternative materials by partially replacing Portland cement with fly ash[11]. Alternative materials that have been developed or tested include reused waste (such as industrial by-products like fly ash or biomass wastes like rice husk ash), alkali materials (such as red mud) and novel binders such as geopolymers or alkali-activated cement [12, 13, 7, 14, 15, 16]. Since these novel binders have low or negative carbon emissions associated with their production, they are sometimes referred to as "green cements" [17]. In most cases, the alternative materials only partially replace clinker. This is advantageous from a regulatory perspective since the existing standardised codes of practice for OPC can be adapted or built upon. It is important that the mechanical properties of alternative cements are similar to (or more

advantageous than) the properties of OPC. Recent studies have found that some OPC novel binder mixtures such as lime-metakaolin have suitable properties [18] and might be preferable to OPC in humid environments [19]. Other novel additives such as silica fume and nano-silica particles improve the properties of OPC [20, 21, 22, 23] and metakaolin-based geopolymers [24, 25]. The main reason geopolymer binders have not yet been more widely adopted by industry is the current lack of regulatory standards backed by long term testing and development [26].

OPC is used in the preparation of mortar for wall rendering/finishing and also in aerated concrete blocks employed as a thermal insulation material [27, 28]. However, aerated OPC does not offer thermal conductivity values comparable to other solutions on the market, such as polymer foam, glass fibres and vacuum insulation panels [29]. Although these materials have very low thermal conductivity, in the range 0.01–0.002 W/(m K) [30, 31], which can help reduce energy consumption, their production is polluting [32, 33] plus they cannot entirely be recycled and have to be disposed of in landfill. Geopolymer binders and OPC-free mixtures have been proposed as alternative insulation materials to OPC-based composites and have shown thermal conductivity values, 0.17–0.35 W/(m K), lower than traditional cement mortar or concrete (0.2–0.8 W/(m K) [34]) although not comparable with insulation materials such as glass fibres or polymers [25].

Life cycle analyses on selected geopolymer binders have found that their use in place of OPC could reduce GHG emissions from the cement industry by 9–64% [35, 7]. However, these life cycle emissions are context and country dependent and often subjected to availability of raw materials [36, 37, 38]. To date, the environmental sustainability of a range of OPC free cement mixtures has not been comparatively explored, nor has there been a comprehensive analysis of properties of alternative cements and their potential to completely replace OPC. Here we consider the carbon reduction that could be

achieved by using seven alternative cementitious materials in place of OPC, evaluate CO_{2eq} gas emissions of OPC and geopolymer production, taking the whole life-cycle into account, including the transport of raw materials and the manufacturing process [1].

The aim of this work is to develop novel *'green'* cementitious materials with superior thermal properties to ordinary Portland cement and low environmental impact. Silica particles, metakaolin and calcium hydroxide are combined in binary or ternary systems and their physical, thermal and mechanical properties are characterised. Thermal performance is calculated in the context of a typical domestic construction and a comparison of GHG emissions for these novel cementitious binders and OPC is presented for the first time in the UK-European context. These OPC-free cements represent an environmental friendly alternative with a high recyclability potential, simple manufacturing process and able to ensure thermal comfort within current international standards. Furthermore, GHG emissions are calculated following a simplified life cycle assessment, which provide a useful decision-making tool to industries or practitioners to rapidly calculate the carbon footprint of novel OPC-free binders.

2. Materials and methods

2.1. Materials

Portland cement samples were prepared using ordinary Portland cement CEM I 42.5-R (CAS number 65997-15-1), commercially available from the Lafarge Cement Group, and deionised water (W). Physico-chemical properties of Portland cement are listed in Table S1 of the Supplementary Material. Cement samples (OPC) were prepared with a liquid to solid (l/s) ratio of 0.3 using a rotary mixer according to BS EN 196-1:2016 and cast into cubic moulds for 24 hours. After 24 hours samples were kept for 28 days at relative humidity of 98 ± 2% and temperature of 21 ± 2 °C in a

nitrogen gas environment to minimise carbonation prior to testing. Novel OPC-free cement samples were prepared using different starting materials. Reagent grade calcium hydroxide, $Ca(OH)_2$ (CAS Number 1305-62-0) and Ludox T50 nano-SiO_2 aqueous suspension (CAS number 7631-86-9) were purchased from Sigma Aldrich. Silica fume (CAS number 69012-64-2), commercially available as SF920D from Elkem Microsilica (Norway), was used. Metakaolin was obtained from calcination of kaolin (China clay type purchased from Imerys UK, CAS number 1332-58-7) at 750 °C over 24 hours, as described by Alonso et al. [39]. Reagent grade sodium hydroxide, NaOH (CAS number 1310-73-2) of nominal concentration 10 M was purchased from Fisher Chemical. Chemical and physical properties of the starting materials (calcium hydroxide (CH), nano-silica (NS), metakaolin (MK), silica fume (SF)) are reported in Table S2 of the Supplementary Material. Given the pozzolanic reactivity of nano-silica and amorphous silica fume, binary mixes using calcium hydroxide and silica (nano-silica or silica fume) were investigated (samples CHI, CHI10, CHNS). Alkali activated binders were prepared mixing metakaolin with calcium hydroxide in different proportions. Sodium hydroxide 10 M was added as an activator (sample MK10, AMK, BMK). Finally metakaolin was mixed with nano-silica and calcium hydroxide, using lower concentration NaOH (1 M) as activator (sample MKNS). Mix proportions and sample identification are listed in Table 1. Fresh paste was cast into cubic moulds and specimens were kept for 28 days at relative humidity of 98 ± 2% and temperature of 21 ± 2 °C in a nitrogen gas environment to minimise carbonation. Sample MK10 was thermally prepared following the methodology of Zhang et al. (2014) for geopolymers [40]. After mixing, specimens were cast into a cubic mold and kept in an oven at 60 °C and atmospheric pressure for 24 hours, then placed in a sealed environment for 28 days at relative humidity of 98 ± 2% and temperature of 21 ± 2 °C.

Table 1: Sample name, mixes and proportion

Sample	OPC	CH	NS	SF	MK	W	NaOH 10 M	NaOH 1 M
			%				l/s ratio	
OPC	100	-	-	-	-	0.3	-	-
CHI	-	75	-	25	-	0.6	-	-
CHI10	-	75	-	25	-	-	0.8	-
MK10	-	-	-	-	100	-	0.8	-
AMK	-	75	-	-	25	-	1	-
BMK	-	66	-	-	33	-	1	-
MKNS	-	10	5	-	85	-	-	1
CHNS	-	50	50	-	-	2	-	-

2.2. Physical, thermal and mechanical properties

After ageing for 28 days samples were removed from the mold and dried at 60 °C to remove pore water and perform mechanical tests and micro-structural analyses. Water removal has an impact on the microstructure, therefore analysis and results presented should be regarded comparatively. Compressive strength testing was performed according to BS EN 196-1:2016, using a uniaxial compressive testing machine at a constant strain rate of 0.4 mm/min until fracture [21, 41]. Three specimens of each composite were tested. The resistance value (R_c) is given in MPa as a mean value of three replicates for each mixing. The heat of hydration was measured using an isothermal calorimeter (I-Cal 4000 HPC, Calmetrix). Fresh paste (*c.* 60 g) was cast into a cylindrical container and placed into the calibrated calorimeter, at a constant temperature of 21 ± 2 °C. The heat flow was recorded over 80 hours. Open porosity (φ) was estimated by measuring the total water content in each sample (in three replicates) after oven-drying at 60 °C and overnight saturation in a vacuum chamber. Open porosity was calculated

using the equations reported in the *Methods* section of the Supplementary Material.

For each sample the laser flash method (LFA) was used to estimate the coefficient of thermal conductivity (λ), given in W/(m·K). A Netzsch instrument 427 LFA was used. Samples of each composition were tested in an argon atmosphere and thermal conductivity was calculated at 25°, 60° and 105 °C according to the BS EN 821-2:1997.

The coefficient of thermal conductivity was estimated using the laser flash method. The specimens were powdered and pelletized using an hydraulic press to make pellets of ⌀12.7 mm and 3 mm thickness. The surface was coated with graphite to minimise reflectance of the laser beam. A pyroceramic standard supplied by Netzsch was analysed and used as a reference material to calculate the specific heat capacity and thermal diffusivity. Thermal conductivity was calculated at 25°, 60° and 105 °C, as a function of the open porosity, using the equations reported in the *Methods* section of the Supplementary Material.

In order to evaluate the insulation properties of these novel cement composites, the thermal transmittance (U) of a typical wall was calculated, using the equations reported in the *Methods* section of the Supplementary Material. An external wall (1 m high and 1 m wide) of standard domestic construction was considered, as shown in Figure 6 (left). The wall consists (from outdoor to indoor) of horizontal bricks (225×112×65 mm BS EN 771-1:2011, λ=0.84 W/(m K)) with a 5 mm layer of cement mortar (λ=1.4 W/(m K), [30]) and externally finished with 18 mm thickness of mortar render (λ=1.4 W/(m K)). Adjacent to the outer brick skin is a 20 mm thick air cavity (λ=0.03 W/(m K)), 9 mm layer of plywood (λ=0.14 W/(m K)), a rock-wool insulation wall of 40 mm thick (λ=0.04 W/m·K, [29]) and a 15 mm thick gypsum plaster board (λ=0.21 W/(mK), [30])finished with 2 mm thick waterproof plaster painting (λ=0.09 W/(m K), [30]). The wall is then finished with an outside mortar render and internal plaster. This is a pattern in the construction that repeats itself every 70 cm in the vertical

direction. Therefore a 1 m wide and 0.7 m high portion of the wall was considered, as it is representative of the entire wall. One-directional heat transfer and constant thermal conductivity values are assumed.

2.3. Powder X-Ray Diffraction and Scanning Electron Microscopy

Powder XRD analyses were performed using a Bruker D8 Advance diffractometer with CuKα radiation over the range 5–60° 2θ, step size of 0.02° 2θ and 0.5 s/step. DiffracEva software from Bruker was used for XRD pattern evaluation and phase identification. Microstructural analysis of samples was carried out using Scanning Electron Microscopy (W-SEM, Hitachi S-3700N and FE-SEM, Hitachi SU6600) with Energy Dispersive Spectroscopy (EDS, Oxford INCA-7260) at an accelerating voltage of 10–15 kV. All samples were resin impregnated, polished and gold coated.

2.4. Greenhouse gas emission assessment

Calculation of the total greenhouse gas emission (GHG), expressed as carbon dioxide equivalent (CO_{2eq}) per 1000 kg of cement produced, takes into account the collective contribution of CH_4, NO_x, SO_x, CO_2 and synthetic gases evolved during production activity, including excavation and transport of raw materials and reagents, and manufacturing. The approach to estimate the total GHG is based on the methodology reported in McLellan et al. (2011) [35] and calculated using the equation 1:

$$GHG_{Tot} = \sum_{i=1}^{n} m_i(d_i e_i + p_i) \tag{1}$$

where GHG_{Tot} is the total greenhouse gas emission ($kg_{CO_{2eq}}$) per ton of material produced, m_i is the fraction of component i, d_i is the distance transported by a given mode of transport (km), e_i is the emission factor for the transportation mode ($kg_{CO_{2eq}}$/(km ton)) and p_i is the emissions per unit mass of component i produced ($kg_{CO_{2eq}}$/ton). The following assumptions were made in the analysis:

1. The calculations were based on the manufacture of 1 ton of Portland cement binder and 1 ton of novel materials in the United Kingdom, using, where possible, UK products, otherwise materials from a typical supply chain.
2. Previously published values for CO_{2eq} emissions from the manufacture of the raw materials were used, and added to the emissions from transport to and within the UK.
3. The emissions due to the addition of water to cement paste are very low (0.271 kg_{CO_2eq}/ton [42]) therefore negligible and not taken into account.
4. Maximum distances and mode of transport are selected as those which maximise CO_{2eq} emissions, because this work adopts the worst-case scenario for CO_{2eq} emissions.
5. Emission factors associated with road transport (e_r) and sea transport (e_s) are respectively 0.09 kg_{CO_2eq}/(km ton) and 0.02 kg_{CO_2eq}/(km ton) [35, 43].
6. Emissions per unit mass of OPC (p_{OPC}) are 750 kg_{CO_2eq}/ton and is produced in mainland UK.
7. Emissions per unit mass of metakaolin (p_{MK}), produced in England and silica fume (p_{SF}), produced in Norway, are respectively 236 kg_{CO_2eq}/ton and 7×10^{-6} kg_{CO_2eq}/ton [44, 35].
8. The manufacture of calcium hydroxide is based on the hydration of calcium oxide, produced in Northern Ireland, (p_{CO}=750 kg_{CO_2eq}/ton) taking into account a correction factor of 0.97 due to the addition of water (p_{CH}=720 kg_{CO_2eq}/ton) as explained in the IPCC Guidelines for national greenhouse gas emissions [45].
9. Sodium hydroxide is produced in Northern Ireland by a chemical process using electrolytic cells. The emissions associated with the production are in the range 1120–1915 kg_{CO_2eq}/ton as reported for a nominal concentration of 16 M [7, 43, 46]. In order to take into account lower sodium hydroxide concentrations, we used a

correction factor of 0.43 and 0.63 respectively for NaOH 1 M and NaOH 10 M on the lowest emission value (p_{NaOH}=1120 $kg_{CO_{2eq}}$/ton), following the principle of the IPCC guidelines [45].

10. Nano-silica solution is manufactured in Germany and the carbon emissions value can be obtained from the manufacture of sodium silicate solution (p_{NS}=386 $kg_{CO_{2eq}}$/ton) [47, 48, 23].

A schematic diagram of mode of transport and distances for each raw material is shown in Figure 2.

3. Results and discussion

3.1. Physical, thermal and mechanical properties

The particle size and the high specific surface area of nano-particles play an important role in the physical and mechanical properties. The measured bulk density (ϱ), matrix density (ϱ_{mat}), open porosity (φ), compressive strength (R_c) results and cumulative heat released values are reported in Table 2. All the mixes show values of bulk density in the range 600–1100 kg/m^3, much lower than standard OPC (1900 kg/m^3). Density and porosity values are in good agreement with literature data on lightweight materials such as calcium silicate boards and aerated concretes [49, 50, 51]. Sample CHI10 shows a higher bulk density and lower porosity due to the greater l/s ratio and the presence of an alkaline activator. Samples MK10, AMK and BMK show decreasing density values directly proportional to the content of metakaolin, from 100% to 66%. On the other hand porosity increases when a lower amount of MK is used (sample MKNS) and higher concentration of nano-silica is used (sample CHNS). Mechanical tests performed on all the samples after 28 days of curing show values of compressive strength, in the range of 1.8–7.8 MPa. Although compressive strength values are not comparable with OPC, they satisfy the resistance requirement for non-loaded structures; results

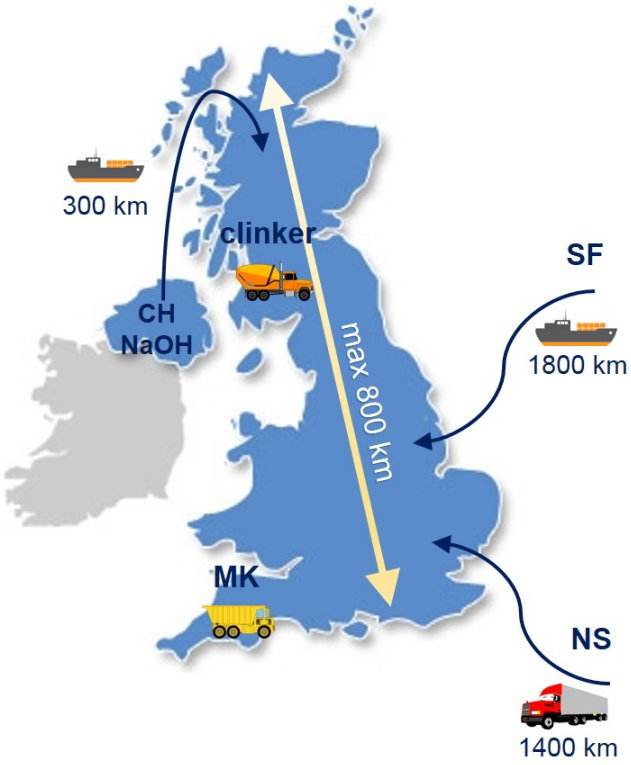

Figure 2: Diagram of transportation mode and average distance for raw materials in and to UK. Silica fume (SF) is supplied from Norway, nano-silica (NS) from Germany, calcium hydroxide (CH) and sodium hydroxide (NaOH) from Northern Ireland (UK), metakaolin (MK) and Portland clinker are available in mainland UK.

are in agreement with the values given for aerated concrete blocks [52, 53] and lime-metakaolin mortars [54, 55]. Isothermal calorimetry was used to measure the heat flow development of the samples at 21 °C. Figure 3 shows the heat flow (in mW/g) of the samples compared to OPC. Since the mixing was done externally, the first peak appears
245 at the very beginning of the measurement for all the samples (Figure 3a); it corresponds to particle wetting and dissolution, the chemical reaction which leads to the formation of hydrated phases. The second peak appears broad and delayed compared to OPC. It corresponds to the polymerisation of dissolved species into new crystal structures. In

sample CHI the first peak converges into a straight horizontal line and no second peak is detected, indicating very low reactivity [56]. Sample CHI10 shows the influence of the alkali-activator, resulting in higher intensity. Specimen CHNS (CH and NS) shows the same trend of mix CHI (CH and SF), with a high first peak converging into a horizontal line. However a second peak is detected as a broad hump at around 20 hours. This is due to the smaller particle size and higher reactivity of NS compared with SF. Sample MK10 shows a high-intensity broad first peak followed by small broad hump associated with the second peak of hydration. Samples AMK and BMK have respectively 75% and 66% of calcium hydroxide content. In sample BMK, the higher content of MK produces a delay in the second peak compared to sample AMK. The peak is higher in intensity from the increased formation of alkaline aluminosilicate due to the greater concentration of dissolved aluminum ions [39]. The cumulative heat released in the first 80 hours was obtained by integrating the heat flow curves and is summarised in Table 2. Except for the mix MK10, with a total heat release of 4.4×10^5 J/kg, in accordance with the work of Zhang et al. [57], all the other mixes show a cumulative energy lower than OPC, due to the lower number of reactants dissolved. Cumulative heat released is detailed in Table 2 and shown in Figure S1 in the Supplementary Material. OPC clinker is a complex mixture of compounds and usually gypsum is added to delay the setting time. Therefore the hydration chemistry of OPC involves more ionic species, resulting in a higher total cumulative heat released.

Table 2: Bulk density (ϱ), matrix density (ϱ_{mat}), open porosity (φ), compressive strength (R_c) and cumulative heat release of all the samples

Sample	ρ	ρ_{mat}	φ	R_c	Heat release
	kg/m^3	kg/m^3	-	MPa	J/g
OPC	1940	2460	0.21	51.2	235
CHI	940	2430	0.61	6.4	44
CHI10	1120	2160	0.48	7.7	211
MK10	1020	2190	0.53	5.2	463
AMK	900	2180	0.59	4.7	75
BMK	850	2020	0.58	6.5	104
MKNS	640	2260	0.72	1.7	51
CHNS	610	2390	0.74	2.2	238

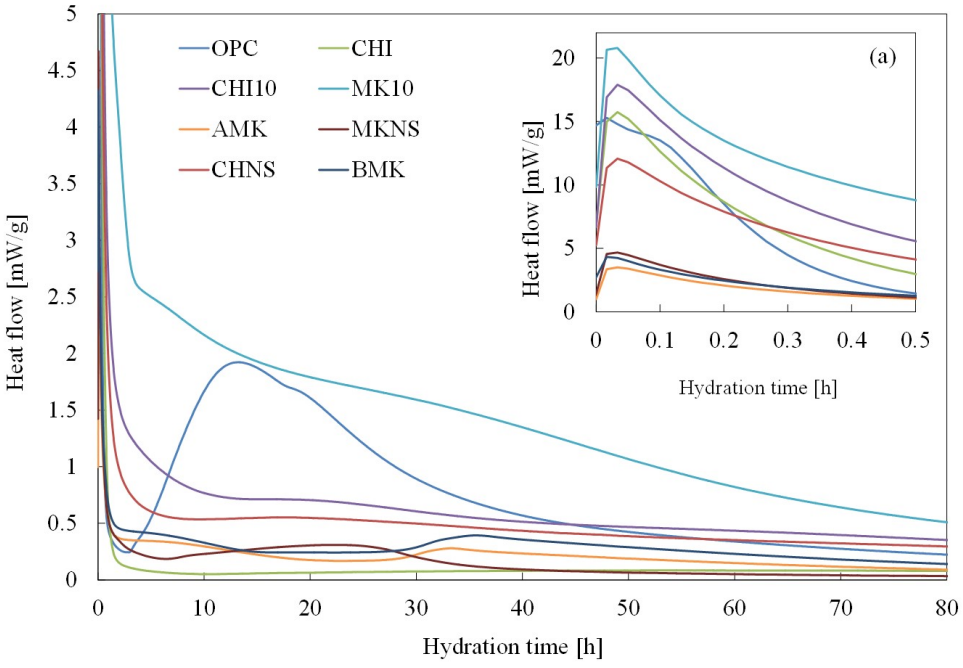

Figure 3: Heat flow measurement for each sample. (a) magnification of the first 30 min of heat flow measurement.

3.2. Powder X-Ray Diffraction and Scanning Electron Microscopy

XRD patterns obtained for the developed materials are presented in Figure S2 in the Supplementary Material, where only the major mineral phases are shown. Samples CHI and CHI10 are mainly crystalline portlandite (P) and semi-crystalline calcium silicate hydrate gel (C-S-H), the most abundant component of hydrated cement paste and responsible for early strength development and hardening [58] or calcium (sodium) silicate hydrate (C-(N)-S-H)[59, 60]. Semi-quantitative analysis of the XRD patterns showed that, despite the high pH, sample CHI10 has 54% C-S-H compared to sample CHI (61%). The added Na^{+} concentration takes Ca^{++} to produce C-N-S-H in addition to the C-S-H produced. Some minor carbonated phases are detected, (calcite, carbon, and sodium carbonate), arising from surface carbonation. In the mixes containing metakaolin and calcium hydroxide (sample AMK, BMK and MKNS), stratlingite (St), calcium aluminate hydrate (C-A-H) and monocarboaluminate (M) phases are detected, in agreement with Silva et al. [19]. Stratlingite is the main hydrate phase responsible for strength development in lime-metakaolin based materials. An increase of metakaolin content from 25% to 35% respectively in samples AMK and BMK results in well defined peaks of stratlingite, and consequently higher compressive strength. Faujasite (F) is the main crystalline compound in sample MK10 along with C-S-H gel, calcium aluminate hydrate and minor stratlingite. In sample MK10, mixing metakaolin with 10 M NaOH solution promotes alkaline activation and leads to the precipitation of sodium aluminum silicate hydrate (N-A-S-H) gel into the mineral structure of faujasite (F) [40, 61]. In sample MKNS, reducing the concentration of the activator from 10 M to 1 M and the addition of calcium hydroxide at ambient temperature results in the precipitation of semi-crystalline calcium aluminate hydrate (C-A-H), the main phase detected. Sample CHNS presents broad humps at *c.* 29° and 32° 2θ, typical of C-S-H gel [62].

As shown in the SEM images, the developed materials present a highly porous

matrix in agreement with the density and porosity values measured. In sample CHI the matrix is mainly semi-crystalline C-S-H whereas the presence of NaOH as alkaline activator in sample CHI10 promotes the formation of C-S-H combined with C-(N)-S-H phases, respectively in Figure 4a and Figure 4b. As shown in XRD patterns, alkali-activation of metakaolin-lime mixes results in formation of calcium aluminate silicate hydrate (stratlingite) and C-S-H (sample BMK, Figure 4c). Figure 4d shows a semi-crystalline C-S-H phase forming a complex plate-like structure in sample CHNS.

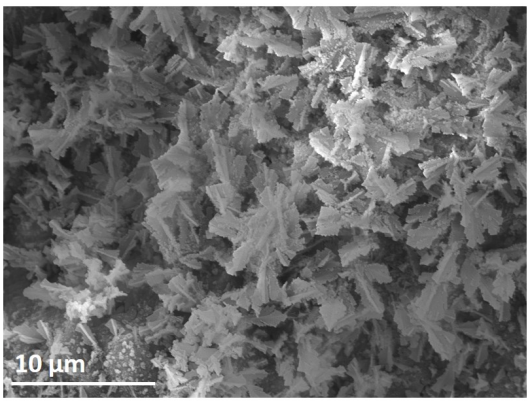

(a) FE-SEM image of sample CHI showing a poorly crystallised C-S-H phase flake-shaped. [Voltage 15 kV].

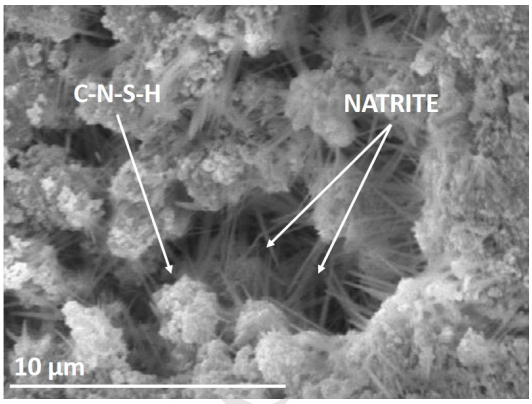

(b) W-SEM image of sample CHI10 showing semi-crystalline C-N-S-H phase and natrite needles. [Voltage 15 kV].

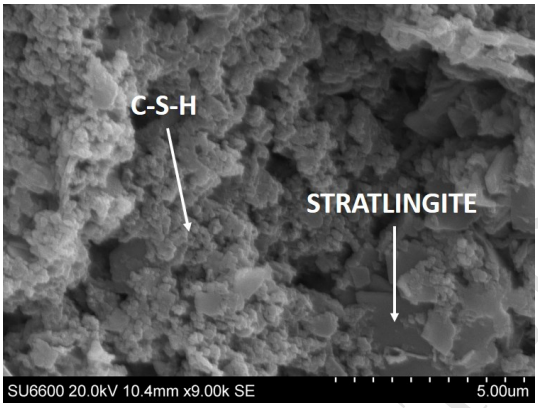

(c) FE-SEM image of sample BMK showing a porous microstructure formed by stratlingite and C-S-H.

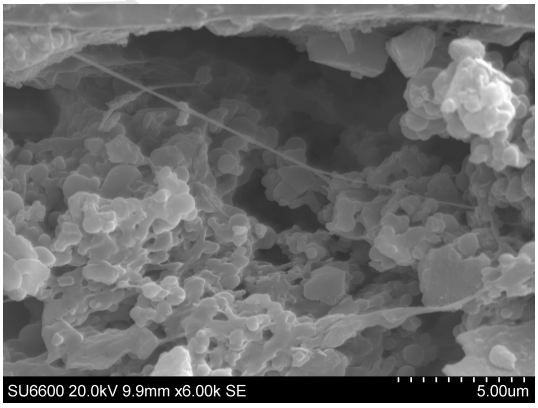

(d) FE-SEM image of sample CHNS showing a porous microstructure formed by plate-like C-S-H phase.

Figure 4: SEM images of (a) sample CHI, (b) sample CHI10, (c) sample BMK, and (d) sample CHNS.

3.3. Thermal conductivity measurements

Thermal conductivity values at 25°, 60° and 105 °C calculated according to equation S5 are shown in Figure 5 and compared to OPC. Values are in the range 0.05–0.26 W/(m K), 50–90% lower than OPC. Samples made mixing metakaolin and sodium

hydroxide (MK10, AMK and BMK) show thermal conductivity values in accordance with Palmero et al. (2015) and Villaquiran-Caicedo et al. (2015) [51, 25]. Furthermore samples show an inversely proportional trend to the content of MK 100%, 75% and 66% wt. respectively. The addition of silica nano-particles has a beneficial effect on the thermal conductivity. Sample MKNS and CHNS in fact show the lowest λ values at 25 °C, 0.055 and 0.088 W/(m K) respectively. These values are typical of insulating materials [63, 30]. This effect is attributed to the nano-silica smaller particle size range and greater surface area, which increases the pore volume (φ=0.7) and decreases the pore-size; the overall consequence is an enhanced phonon scattering effect which reduces heat transfer [64]. Samples made by mixing CH and SF, either with water or alkali-actived show a different thermal behaviour: while sample CHI has a thermal conductivity value (λ=0.09 W/(m K)) similar to CHNS, sample CHI10 has a higher λ, suggesting that the alkali-activator (NaOH, 10 M) contributes to the reduction of porosity and decreases the thermal transmittance. As shown in XRD patterns, sample CHI contains C-S-H and portlandite, whereas CHI10 is made of C-S-H, natrite and portlandite, bound together in a denser and less porous matrix (*c.* 20% less than CHI).

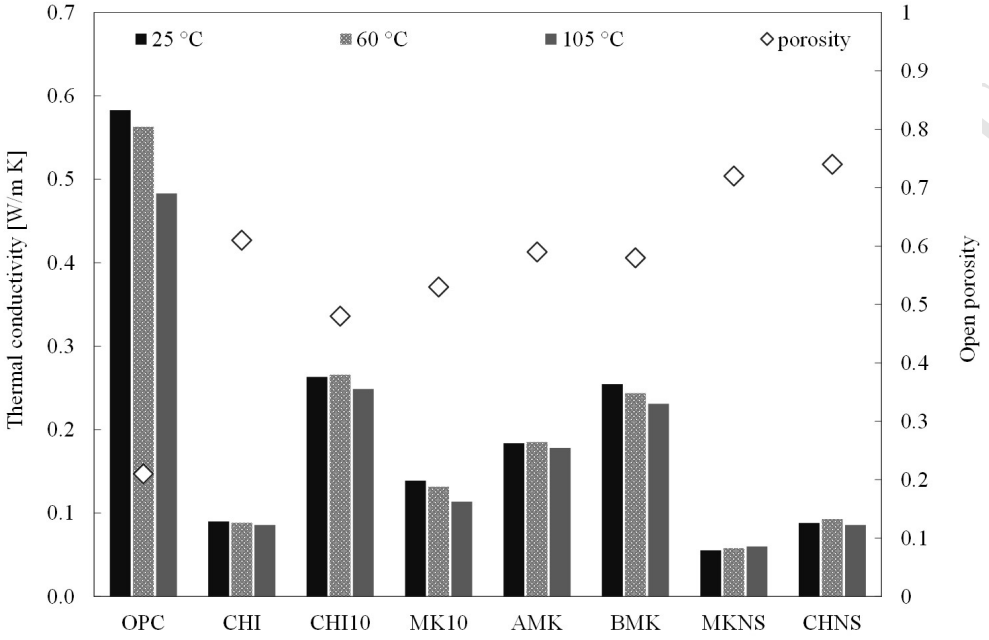

Figure 5: Thermal conductivity of samples at 25°, 60° and 105 °C and porosity values.

Thermal transmittance (U-value) for the typical wall (Figure 6) was calculated to be 0.32 W/(m K), using equations reported in the *Methods* section of the Supplementary Material. Building Regulation 2013 in England and Wales for refurbishment of existing buildings (domestic and non-domestic use) requires values less than 0.30 W/(m K). The application of a layer of novel cementitious material can contribute to the reduction of the total transmittance below the limit imposed by building regulations, using materials of relatively simple manufacture. The U-value was then calculated taking into account an additional layer of developed material placed in between the bricks and the air cavity. The thickness was chosen in order to minimise the total transmittance below the limit of the building regulations. Thickness values of all the mixes are summarised in Table 3. The thickness of insulation material layers used in the construction industry is in the range of 30–100 mm (e.g. glass fiber, rock-wool or polymeric foam[30]). Here, a 20 mm layer of mix MKNS is required to reduce the total transmittance by 10%, as shown

335 in Figure 6. Conventional insulation materials such as rock-wool, polystyrene or glass fibres, are usually placed in layers of approximately 40–80 mm [31, 65].

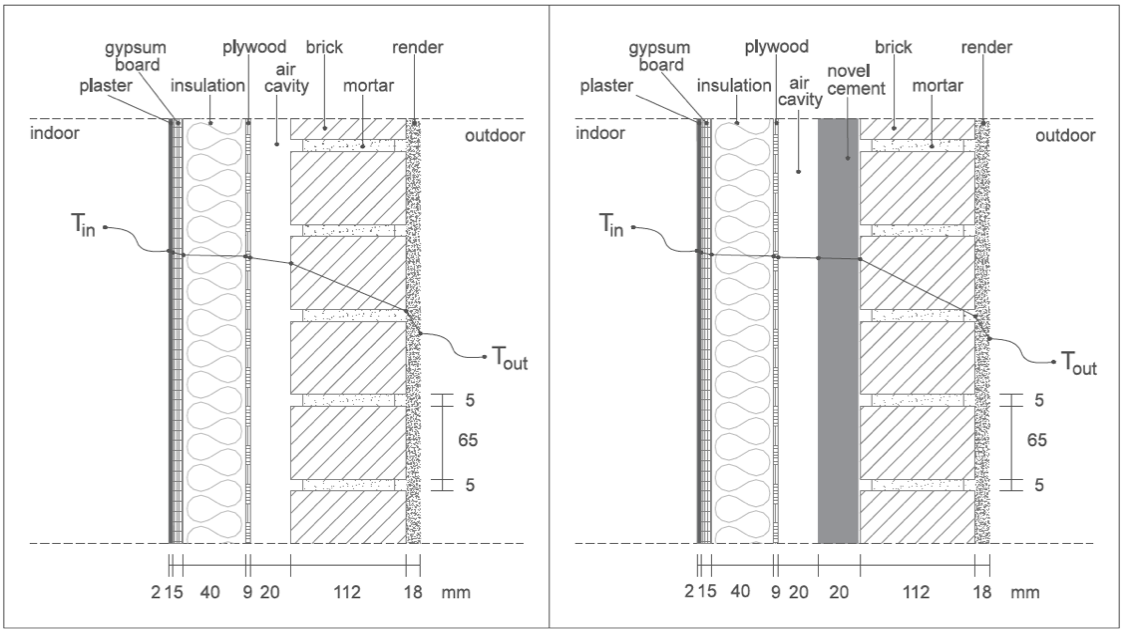

Figure 6: Typical external composite brick wall of domestic building in United Kingdom. (Left: Wall section and temperature (T)profile. Right: Wall-section including a layer of MKNS and temperature profile)

3.4. Life cycle emissions

Previous studies have addressed the need to meet thermal requirements, using high thermal resistant polymers or composites, but the carbon footprint associated to their 340 manufacture is often overlooked [63, 66]). The estimated CO_{2eq} emissions (GHG_i) for each of the seven cementitious material are reported in Figure 7 and compared to OPC. These present the 'worst case scenario', and so the actual CO_{2eq} emissions would likely be lower than those reported here. The carbon footprint of each component material is shown in Figure 7a. The calculated values are similar to previously published

Table 3: Minimum thickness of novel cement to achieve U-value ≤ 0.29 W/(m^2 K)

Sample	minimum thickness mm
CHI	30
CHI10	80
MK10	50
AMK	60
BMK	80
MKNS	20
CHNS	30

estimates for geopolymer binders and concrete in different contexts [35, 7, 43, 46]. The results show that all types of novel cements studied here have lower embedded carbon compared to OPC. For example, sample MKNS has the lowest CO_{2eq} emissions associated with its manufacture, estimated to be half the emissions from OPC. Sample AMK, which has the highest embedded carbon among the novel cements, still has 20% lower CO_{2eq} than OPC. The selected raw materials, their world-wide availability coupled with minimum manufacturing make these novel binders environmentally competitive compared to traditional insulators (e.g. 1 ton of extruded polystyrene is responsible for 1180 $kg_{CO_{2eq}}$) [32]. NaOH and CH are the most common ingredients of the alternative cements tested here, and the embedded carbon in these materials is similar to clinker (Figure 7a). Thus, it is the relative proportion of low carbon materials such as SF, MK and NS which determine the overall carbon footprint for each cement. The major energy expended in the manufacture of NaOH occurs in the electrolysis process followed by cooling, which has a large electricity requirement. However, recent findings have

proven that natural highly alkaline materials could be used, with comparatively high mechanical performance [16]. CH is produced by calcination of calcium carbonate followed by hydration. The CO_2 footprint of both materials could be reduced if they were produced using alternative source of energy for the electricity required (e.g. wind turbine, nuclear energy, photovoltaic energy for the manufacture of NaOH) or using bio-mass or other green fuel in the pyroprocessing of calcium carbonate.

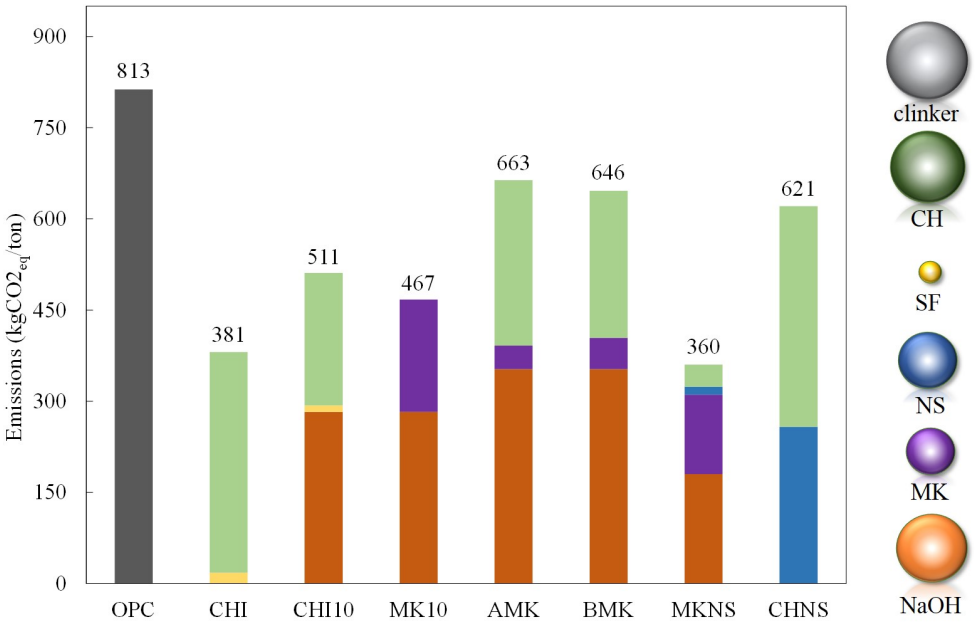

Figure 7: Total GHG emission and contribution of each raw material for all the mixes. (a) Bubbles indicate the single component in each mix and the size indicates the GHG emission associated: clinker (750 $kg_{CO_{2eq}}$/ton), CH (720 $kg_{CO_{2eq}}$/ton), SF (0.01 $kg_{CO_{2eq}}$/ton), NS (390 $kg_{CO_{2eq}}$/ton), MK (236 $kg_{CO_{2eq}}$/ton), NaOH 10 M (700 $kg_{CO_{2eq}}$/ton), NaOH 1 M (481 $kg_{CO_{2eq}}$/ton).

3.5. Environmental impact

The low thermal conductivity of the novel cements also present an environmentally sustainable alternative for purposes such as wall cladding. Improving insulation in homes and buildings is an important aspect of reducing thermal energy loss and thus in

turn reducing energy consumption. These innovative binders are also highly recyclable compared to conventional insulating components such as polymeric foams, polystyrene, polyurethane, rock-wool or vacuum insulation panels. They could be re-used in the building industry as construction and demolition waste (CDW), as intended by the European Waste Framework Directive 2008/98/EC and the EU Framework Programme for Research and Innovation Horizon 2020: '*incorporation up to c. 80% of recycled CDW material to decrease the content of Portland cement used and consequently reduce the amount of waste to be placed in landfill'*. These innovative cements are more environmentally friendly than OPC and other polymeric plastic insulators, and offer an environmental friendly alternative to traditional materials. They require less manufacturing and processing and the raw materials and reagents are readily available, which is important to consider for large-scale production.

Thus, although novel cements cannot replace OPC in all applications, they offer an environmentally sustainable alternative for several applications, and there is significant potential for these materials to contribute towards the decarbonisation of the cement industry.

4. Conclusions

In this study low-carbon cementitious materials have been developed and characterised. Metakaolin, silica fume, nano-silica and calcium hydroxide were combined at different ratios to produce 'green' binders for construction industry. Physical and mechanical properties were investigated. Compressive strength values (in the range 2–7 MPa) are typical of non-structural cements (mortars, rendering cements, etc.); density and porosity measurements show that these materials could be used in construction industry as functional building elements. Pozzolanic activity was detected by isothermal calorimetry and hydrated phases (calcium/aluminum silicate hydrate, fauj-

asite, stratlingite) were found in XRD diffractograms. SEM images give an insight to the micro-structure, with the presence of semi-crystalline phases (C-S-H) and highly porous matrix, in agreement with the porosity measurements (0.48–0.74). Samples present thermal conductivity (0.05–0.26 W/m·K), in the range of conventional insulating materials. While previous studies have focused their attention on solely physical properties of OPC-free cements and geopolymers, here we brought together innovative materials able to satisfy thermal performance requirements within environmental standards. In facts, the addition of a 20 mm layer of sample MKNS to an external wall of existing housing, contributes to 10% decrease in thermal transmittance, as required by the Building Regulation 2013 in England and Wales. The environmental impact of the newly developed materials was assessed estimating the greenhouse gas emission associated to the manufacturing and production; all the sample have a carbon footprint up to 23–55% lower than OPC. These materials are 'cleaner' than OPC and help to reduce CO_{2eq} emissions. The life cycle analysis presented here is simplistic, and more detailed life cycle and cost analyses should be the subject of future research to fully understand the economic impact of those materials in replacing OPC. However, the methodology adopted provides the basis for implementing a decision-making tool that can advise on, or scope in, low-carbon options before a more resource intensive life cycle assessment approach is applied. It will be therefore useful to construction companies or private developers intended to develop non-conventional building materials (e.g. geopolymers, alkali-activated cements), not yet regulated by law or international standards.

Supplementary Material

The following data are available free of charge.

- Table S1–S2: Details of physico-chemical properties of starting materials.

- Figure S1: Cumulative heat release as specific energy.
- Figure S2: X-Ray diffractograms of hydrated mixes.
- Methods for the calculation of open porosity, thermal conductivity and transmittance.

Acknowledgement

This work is supported by UK Engineering and Physical Sciences Research Council, (EPSRC Grant No. EP/L014041/1 - DISTINCTIVE Consortium - Decommissioning, Immobilisation and Storage soluTIons for NuClear wasTe InVEntories). Data associated with research published in this article is accessible at: http://dx.doi.org/10.15129/b74bc130-e22d-4043-983b-9823139666f2

References

[1] M. S. Imbabi, C. Carrigan, S. McKenna, Trends and developments in green cement and concrete technology, International Journal of Sustainable Built Environment 1 (2) (2012) 194–216. doi:10.1016/j.ijsbe.2013.05.001.
URL http://dx.doi.org/10.1016/j.ijsbe.2013.05.001

[2] M. Schneider, M. Romer, M. Tschudin, H. Bolio, Sustainable cement productionpresent and future, Cement and Concrete Research 41 (7) (2011) 642–650. doi:10.1016/j.cemconres.2011.03.019.
URL http://www.sciencedirect.com/science/article/pii/S0008884611000950

[3] E. Benhelal, G. Zahedi, E. Shamsaei, A. Bahadori, Global strategies and potentials to curb {CO}2 emissions in cement industry, Journal of Cleaner Production

51 (0) (2013) 142–161. doi:10.1016/j.jclepro.2012.10.049.
URL http://www.sciencedirect.com/science/article/pii/S0959652612006129

[4] World Business Council for Sustainable Development, I. E. A. IEA, Cement roadmap, Tech. rep. (2010).

[5] D. A. Salas, A. D. Ramirez, C. R. Rodríguez, D. M. Petroche, A. J. Boero, J. Duque-Rivera, Environmental impacts, life cycle assessment and potential improvement measures for cement production: A literature review, Journal of Cleaner Production 113 (2016) 114–122. doi:10.1016/j.jclepro.2015.11.078.

[6] A. Hasanbeigi, L. Price, H. Lu, W. Lan, Analysis of energy-efficiency opportunities for the cement industry in Shandong Province, China: A case study of 16 cement plants, Energy 35 (8) (2010) 3461–3473. doi:10.1016/j.energy.2010.04.046.
URL http://dx.doi.org/10.1016/j.energy.2010.04.046

[7] L. K. Turner, F. G. Collins, Carbon dioxide equivalent (CO2-e) emissions: A comparison between geopolymer and OPC cement concrete, Construction and Building Materials 43 (2013) 125–130. doi:10.1016/j.conbuildmat.2013.01.023.
URL http://www.sciencedirect.com/science/article/pii/S0950061813000871

[8] A. Hienola, J.-p. Pietikäinen, D. O. Donnell, A.-i. Partanen, H. Korhonen, The role of anthropogenic aerosol emission reduction in achieving the Paris Agreement 's objective, Geophysical Research Abstracts 19.

[9] WBCSD, CO2 and Energy Accounting and Reporting Standard for the Cement Industry, Tech. Rep. May (2011).

[10] Various, Industrial Decarbonisation & Energy Efficiency Roadmaps to 2050 - Cement, Tech. rep., Department for Business, Innovation & Skills and Department of Energy & Climate Change (2015).

[11] R. Kajaste, M. Hurme, Cement industry greenhouse gas emissions - Management options and abatement cost, Journal of Cleaner Production 112 (2016) 4041–4052. doi:10.1016/j.jclepro.2015.07.055.
URL http://dx.doi.org/10.1016/j.jclepro.2015.07.055

[12] H. Rostami, W. Brendley, Alkali ash material: A novel fly ash-based cement, Environmental Science and Technology 37 (15) (2003) 3454–3457. doi:10.1021/es026317b.

[13] M. Cruz-Yusta, I. Mármol, J. Morales, L. Sánchez, Use of olive biomass fly ash in the preparation of environmentally friendly mortars, Environmental Science and Technology 45 (16) (2011) 6991–6996. doi:10.1021/es200968a.

[14] Y. Wu, J. Y. Wang, P. J. M. Monteiro, M. H. Zhang, Development of ultra-lightweight cement composites with low thermal conductivity and high specific strength for energy efficient buildings, Construction and Building Materials 87 (2015) 100–112. doi:10.1016/j.conbuildmat.2015.04.004.
URL http://dx.doi.org/10.1016/j.conbuildmat.2015.04.004

[15] P. Sturm, G. J. G. Gluth, H. J. H. Brouwers, H. C. Kühne, Synthesizing one-part geopolymers from rice husk ash, Construction and Building Materials 124 (2016) 961–966. doi:10.1016/j.conbuildmat.2016.08.017.
URL http://dx.doi.org/10.1016/j.conbuildmat.2016.08.017

[16] Q. Nie, W. Hu, T. Ai, B. Huang, X. Shu, Q. He, Strength properties of geopolymers derived from original and desulfurized red mud cured at ambient tempera-

ture, Construction and Building Materials 125 (2016) 905–911. doi:10.1016/j.conbuildmat.2016.08.144.
URL http://dx.doi.org/10.1016/j.conbuildmat.2016.08.144

[17] T. Hemalatha, M. Mapa, N. George, S. Sasmal, Physico-chemical and mechanical characterization of high volume fly ash incorporated and engineered cement system towards developing greener cement, Journal of Cleaner Production 125 (2016) 268–281. doi:10.1016/j.jclepro.2016.03.118.
URL http://dx.doi.org/10.1016/j.jclepro.2016.03.118

[18] A. Gameiro, A. Santos Silva, R. Veiga, A. Velosa, Hydration products of limemetakaolin pastes at ambient temperature with ageing, Thermochimica Acta 535 (2012) 36–41. doi:10.1016/j.tca.2012.02.013.
URL http://www.sciencedirect.com/science/article/pii/S0040603112000585

[19] A. S. Silva, A. Gameiro, J. Grilo, R. Veiga, A. Velosa, Long-term behavior of limemetakaolin pastes at ambient temperature and humid curing condition, Applied Clay Science 88 (2014) 49–55. doi:10.1016/j.clay.2013.12.016.

[20] K. N. Yu, R. V. Balendran, S. Y. Koo, T. Cheung, Silica fume as a radon retardant from concrete, Environmental Science and Technology 34 (11) (2000) 2284–2287. doi:10.1021/es991134j.

[21] F. Sanchez, C. Ince, Microstructure and macroscopic properties of hybrid carbon nanofiber/silica fume cement composites, Composites Science and Technology 69 (7-8) (2009) 1310–1318. doi:10.1016/j.compscitech.2009.03.006.
URL http://www.sciencedirect.com/science/article/pii/S0266353809001079

[22] P. Aggarwal, R. P. Singh, Y. Aggarwal, Use of nano-silica in cement based materialsA review, Cogent Engineering 2 (1) (2015) 1078018. doi:10.1080/23311916.2015.1078018.
URL http://www.tandfonline.com/doi/abs/10.1080/23311916.2015.1078018?src=recsys

[23] A. Lazaro, Q. Yu, H. Brouwers, 4 Nanotechnologies for sustainable construction, Sustainability of Construction Materials (2016) 55–78doi:10.1016/B978-0-08-100370-1.00004-4.

[24] K. Gao, K.-L. Lin, D. Wang, C.-L. Hwang, B. L. Anh Tuan, H.-S. Shiu, T.-W. Cheng, Effect of nano-SiO2 on the alkali-activated characteristics of metakaolin-based geopolymers, Construction and Building Materials 48 (2013) 441–447. doi:10.1016/j.conbuildmat.2013.07.027.
URL http://www.sciencedirect.com/science/article/pii/S0950061813006417

[25] M. A. Villaquiran-Caicedo, R. M. de Gutierrez, S. Sulekar, C. Davis, J. C. Nino, Thermal properties of novel binary geopolymers based on metakaolin and alternative silica sources, Applied Clay Science 118 (2015) 276–282. doi:10.1016/j.clay.2015.10.005.
URL http://dx.doi.org/10.1016/j.clay.2015.10.005

[26] C. Heidrich, J. Sanjayan, M. L. Berndt, S. Foster, Pathways and barriers for acceptance and usage of geopolymer concrete in mainstream construction, in: 2015 World of Coal Ash (WOCA) Conference in Nashville, Nashville, 2015.

[27] A. Ahmed, A. Fried, Flexural strength of low density blockwork, Construction and Building Materials 35 (2012) 516–520. doi:10.1016/j.conbuildmat.2012.04.

082.
URL http://dx.doi.org/10.1016/j.conbuildmat.2012.04.082

[28] Z. Zhang, J. L. Provis, A. Reid, H. Wang, Geopolymer foam concrete: An emerging material for sustainable construction, Construction and Building Materials 56 (2014) 113–127. doi:10.1016/j.conbuildmat.2014.01.081.
URL http://www.sciencedirect.com/science/article/pii/S0950061814001160

[29] M. S. Al-homoud, Performance characteristics and practical applications of common building thermal insulation materials, Building and Environment 40 (2005) 353–366. doi:10.1016/j.buildenv.2004.05.013.

[30] K. Cho, Y. Hong, J. Seo, Assessment of the economic performance of vacuum insulation panels for housing projects, Energy and Buildings 70 (2014) 45–51. doi:10.1016/j.enbuild.2013.11.073.
URL http://dx.doi.org/10.1016/j.enbuild.2013.11.073

[31] F. Aldawi, F. Alam, Residential Building Wall Systems, Elsevier Inc., 2016. doi:10.1016/B978-0-12-802397-6.00008-7.
URL http://linkinghub.elsevier.com/retrieve/pii/B9780128023976000087

[32] A. M. Papadopoulos, E. Giama, Environmental performance evaluation of thermal insulation materials and its impact on the building, Building and Environment 42 (5) (2007) 2178–2187. doi:10.1016/j.buildenv.2006.04.012.

[33] S. Proietti, U. Desideri, P. Sdringola, F. Zepparelli, Carbon footprint of a reflective foil and comparison with other solutions for thermal insulation in building envelope,

Applied Energy 112 (2013) 843–855. doi:10.1016/j.apenergy.2013.01.086.
URL http://dx.doi.org/10.1016/j.apenergy.2013.01.086

[34] A. G. Loudon, The thermal properties of lightweight concretes, International Journal of Cement Composites and Lightweight Concrete 1 (2) (1979) 71–85. doi:10.1016/0262-5075(79)90013-7.

[35] B. C. McLellan, R. P. Williams, J. Lay, A. van Riessen, G. D. Corder, Costs and carbon emissions for geopolymer pastes in comparison to ordinary portland cement, Journal of Cleaner Production 19 (9-10) (2011) 1080–1090. doi:10.1016/j.jclepro.2011.02.010.
URL http://www.sciencedirect.com/science/article/pii/S0959652611000680

[36] F. N. Stafford, A. C. Dias, L. Arroja, J. A. Labrincha, D. Hotza, Life cycle assessment of the production of Portland cement: A Southern Europe case study, Journal of Cleaner Production 126 (2016) 159–165. doi:10.1016/j.jclepro.2016.02.110.

[37] F. N. Stafford, F. Raupp-Pereira, J. A. Labrincha, D. Hotza, Life cycle assessment of the production of cement: A Brazilian case study, Journal of Cleaner Production 137 (2016) 1293–1299. doi:10.1016/j.jclepro.2016.07.050.

[38] L. Moretti, S. Caro, Critical analysis of the Life Cycle Assessment of the Italian cement industry, Journal of Cleaner Production 152 (2017) 198–210. doi:10.1016/j.jclepro.2017.03.136.
URL http://dx.doi.org/10.1016/j.jclepro.2017.03.136

[39] S. Alonso, A. Palomo, Alkaline activation of metakaolin and calcium hydroxide mixtures: influence of temperature, activator concentration and solids ratio,

Materials Letters 47 (1-2) (2001) 55–62. doi:10.1016/S0167-577X(00)00212-3.
URL http://www.sciencedirect.com/science/article/pii/S0167577X00002123

[40] J. Zhang, Y. He, Y.-p. Wang, J. Mao, X.-m. Cui, Synthesis of a self-supporting faujasite zeolite membrane using geopolymer gel for separation of alcohol/water mixture, Materials Letters 116 (2014) 167–170. doi:10.1016/j.matlet.2013.11.008.
URL http://www.sciencedirect.com/science/article/pii/S0167577X13015255

[41] Q. Lin, X. Lan, Y. Li, Y. Ni, C. Lu, Y. Chen, Z. Xu, Preparation and characterization of novel alkali-activated nano silica cements for biomedical application., Journal of biomedical materials research. Part B, Applied biomaterials 95 (2) (2010) 347–56. doi:10.1002/jbm.b.31722.
URL http://www.ncbi.nlm.nih.gov/pubmed/20878921

[42] E. Reffold, F. Leighton, F. Choudhury, P. S. Rayner, Greenhouse gas emissions of water supply and demand management options, Tech. rep., Environment Agency (2008).

[43] A. Mellado, C. Catalán, N. Bouzón, M. V. Borrachero, J. M. Monzó, J. Payá, Carbon footprint of geopolymeric mortar: Study of the contribution of the alkaline activating solution and assessment of an alternative route, RSC Advances 4 (2014) 23846–23852. doi:10.1039/c4ra03375b.
URL http://www.scopus.com/inward/record.url?eid=2-s2.0-84902480034{&}partnerID=40{&}md5=1285a2ae152afed70fe639271693f542

[44] P. Duxson, J. L. Provis, G. C. Lukey, J. S. J. van Deventer, The role of inorganic

polymer technology in the development of 'green concrete', Cement and Concrete Research 37 (12) (2007) 1590–1597. doi:10.1016/j.cemconres.2007.08.018.

[45] IPCC, Chapter 2: Mineral Industry Emissions, 2006 IPCC Guidelines for National Greenhouse Gas Inventories 3 (2006) 40.
URL http://www.ipcc-nggip.iges.or.jp/public/2006gl/pdf/3{_}Volume3/V3{_}2{_}Ch2{_}Mineral{_}Industry.pdf

[46] C. C. S. Chan, D. Thorpe, M. Islam, An evaluation carbon footprint in fly ash based geopolymer cement and ordinary Portland cement manufacture, IEEE International Conference on Industrial Engineering and Engineering Management 2016-Janua (1) (2016) 254–259. doi:10.1109/IEEM.2015.7385647.

[47] EU, Reference document on best available techniques for the manufacture of large volume inorganic chemicals - Silica and others, European Commission BREF - LVI (August) (2007) 1–711.
URL http://eippcb.jrc.ec.europa.eu/reference/lvic-aaf.html

[48] A. Lazaro, G. Quercia, H. J. H. Brouwers, J. W. Geus, Synthesis of a Green Nano-Silica Material Using Beneficiated Waste Dunites and Its Application in Concrete, World Journal of Nano Science and Engineering 03 (03) (2013) 41–51. doi:10.4236/wjnse.2013.33006.
URL http://www.scirp.org/journal/PaperInformation.aspx?PaperID=36671

[49] A. Hamilton, C. Hall, Physicochemical Characterization of a Hydrated Calcium Silicate Board Material, Journal of Building Physics 29 (1) (2005) 9–19. doi:10.1177/1744259105053280.
URL http://jen.sagepub.com/cgi/doi/10.1177/1744259105053280

[50] O. Ünal, T. Uygunolu, A. Yildiz, Investigation of properties of low-strength lightweight concrete for thermal insulation, Building and Environment 42 (2) (2007) 584–590. doi:10.1016/j.buildenv.2005.09.024.

[51] P. Palmero, A. Formia, P. Antonaci, S. Brini, J. M. Tulliani, Geopolymer technology for application-oriented dense and lightened materials. Elaboration and characterization, Ceramics International 41 (10) (2015) 12967–12979. doi:10.1016/j.ceramint.2015.06.140.
URL http://dx.doi.org/10.1016/j.ceramint.2015.06.140

[52] K. S. Al-Jabri, A. W. Hago, A. S. Al-Nuaimi, A. H. Al-Saidy, Concrete blocks for thermal insulation in hot climate, Cement and Concrete Research 35 (8) (2005) 1472–1479. doi:10.1016/j.cemconres.2004.08.018.

[53] T. M. Prakash, B. G. Naresh, B. G. Karisiddappa, S. Raghunath, Properties of Aerated (Foamed) Concrete Blocks, International Journal of Scientific & Engineering Research 4 (1) (2013) 1–5.

[54] J. Grilo, A. Santos Silva, P. Faria, A. Gameiro, R. Veiga, A. Velosa, Mechanical and mineralogical properties of natural hydraulic lime-metakaolin mortars in different curing conditions, Construction and Building Materials 51 (2014) 287–294. doi:10.1016/j.conbuildmat.2013.10.045.

[55] A. Gameiro, A. Santos Silva, P. Faria, J. Grilo, T. Branco, R. Veiga, A. Velosa, Physical and chemical assessment of limemetakaolin mortars: Influence of binder:aggregate ratio, Cement and Concrete Composites 45 (2014) 264–271. doi:10.1016/j.cemconcomp.2013.06.010.

[56] S. Nath, S. Maitra, S. Mukherjee, S. Kumar, Microstructural and morphological

evolution of fly ash based geopolymers, Construction and Building Materials 111 (2016) 758–765. doi:10.1016/j.conbuildmat.2016.02.106.

[57] Z. Zhang, H. Wang, J. L. Provis, F. Bullen, A. Reid, Y. Zhu, Quantitative kinetic and structural analysis of geopolymers. Part 1. the activation of metakaolin with sodium hydroxide, Thermochimica Acta 539 (2012) 23–33. doi:10.1016/j.tca.2012.03.021.
URL http://dx.doi.org/10.1016/j.tca.2012.03.021

[58] H. Taylor, Cement chemistry, 2nd Edition, Vol. 20, 1998. doi:10.1016/S0958-9465(98)00023-7.

[59] L. Gomez-zamorano, M. Balonis, B. Erdemli, N. Neithalat, Structure , Composition and Thermochemical Properties of C-(N)-S-H and N-A-S-H Gels, in: 1st International Conference on Grand Challenges in Construction Materials, 2016, pp. 1–9.

[60] L. Gomez-Zamorano, M. Balonis, B. Erdemli, N. Neithalath, G. Sant, C-(N)-S-H and N-A-S-H gels: Compositions and solubility data at 25C and 50C, Journal of the American Ceramic Society (May 2016) (2017) 2700–2711. doi:10.1111/jace.14715.

[61] L. Reig, L. Soriano, M. Borrachero, J. Monzó, J. Payá, Influence of calcium aluminate cement (CAC) on alkaline activation of red clay brick waste (RCBW), Cement and Concrete Composites 65 (2016) 177–185. doi:10.1016/j.cemconcomp.2015.10.021.

[62] K. Garbev, M. Bornefeld, G. Beuchle, P. Stemmermann, Cell Dimensions and Composition of Nanocrystalline Calcium Silicate Hydrate Solid Solutions. Part 2: X-Ray and Thermogravimetry Study, Journal of the American Ceramic Society

91 (9) (2008) 3015–3023. doi:10.1111/j.1551-2916.2008.02601.x.
URL http://doi.wiley.com/10.1111/j.1551-2916.2008.02601.x

[63] J. Fricke, U. Heinemann, H. P. Ebert, Vacuum insulation panels-From research to market, Vacuum 82 (7) (2008) 680–690. doi:10.1016/j.vacuum.2007.10.014.

[64] F. X. Alvarez, D. Jou, A. Sellitto, Pore-size dependence of the thermal conductivity of porous silicon: A phonon hydrodynamic approach, Applied Physics Letters 97 (3) (2010) 1–4. doi:10.1063/1.3462936.

[65] J. Bull, A. Gupta, D. Mumovic, J. Kimpian, Life cycle cost and carbon footprint of energy efficient refurbishments to 20th century UK school buildings, International Journal of Sustainable Built Environment 3 (1) (2014) 1–17. doi:10.1016/j.ijsbe.2014.07.002.
URL http://www.sciencedirect.com/science/article/pii/S2212609014000387

[66] M. Alam, H. Singh, S. Brunner, C. Naziris, Experimental characterisation and evaluation of the thermo-physical properties of expanded perlite - Fumed silica composite for effective vacuum insulation panel (VIP) core, Energy and Buildings 69 (2014) 442–450. doi:10.1016/j.enbuild.2013.11.027.
URL http://dx.doi.org/10.1016/j.enbuild.2013.11.027

- Green cements high in porosity and very low in thermal conductivity are developed.
- They are a low-carbon alternative to traditional insulation materials and mortars.
- A simplified GHG emissions estimation method has been proposed in the UK context.